Explicit solution of functionally graded plates with respect to law indexes based on a variable separation method

P. Vidal, L. Gallimard, O. Polit, E. Valot

Version of Record: https://www.sciencedirect.com/science/article/pii/S0997753822001309
Manuscript_4a0f3ee87c36b1ef3ffbf5e123a4b6a8

Explicit solution of functionally graded plates with respect to law indexes based on a variable separation method

P. Vidal[a,*], L. Gallimard[a], O. Polit[a], E. Valot[a]

[a]*LEME, UPL, Univ Paris Nanterre, F92410 Ville d'Avray - France*

Abstract

The present work aims at building an explicit solution with respect to Functionally Graded Material (FGM) parameter for plate structures. For that, the displacement field is written under a separated variables form: the in-plane coordinates x, y, the transverse coordinate z and the material parameter chosen beforehand. This choice yields to a non-linear problem that can be solved by an iterative process based on a classical fixed point strategy. One 2D and two 1D linear problems are solved alternatively. In the thickness direction, a fourth-order expansion in each layer is considered. For the in-plane description, classical Finite Element method is used. The number of unknowns is reduced compared to layerwise approach and no additional computation has to be performed for different values of the material parameter. Numerical tests encountered in the literature are provided to show the accuracy of the present method. Different types of FGM law, configurations and slenderness ratios are considered. Comparing with reference solutions and models available in literature, it can be concluded that the model gives very accurate results for a very attractive computational cost.

Keywords: Functionally graded materials, explicit solution, material parameter, Separation of variables, Finite Element

1. Introduction

Functionally Graded Material (FGM) is a class of composite materials that has continuous and smooth variation of material properties from one surface to another, and thus

*Corresponding author
Email address: philippe.vidal@parisnanterre.fr (P. Vidal)

eliminates the stress concentration found in laminated composites, for instance. Other attractive aspects are also summarized in [1], increasing the use of such materials. Thus, it calls for the development of efficient numerical tools allowing us to predict accurate displacements / stresses for design purpose or in an optimization process involving many computations.

Over the past years, the interest for the modeling of plate structures made of FGM has substantially increased. Different approaches can be considered. The classical way consists in using 3D models, as in [2–4] with an application for FGM and sandwich structures. The main drawback remains the computational cost. Consequently, some 2D models belonging to the Equivalent Single Layer model (ESL) have been developed. A low number of generalized unknowns is used as the displacements are written through the whole thickness of the plate. In this family, Classical Laminate Theory (CLT) [5] and First-order Shear Deformation Theory (FSDT) [6] have some well-known limitations (thick structures, needs of the use of a shear correction factor ...). Thus, some Higher-order Shear Deformation Theory (HSDT) models have been proposed. The representation of the transverse shear stresses has been improved considering different expressions of the so-called strain shape functions: polynomial [7, 6, 8–10], trigonometric [9, 11], inverse trigonometric [12], specified [13, 14] functions. But, it has been established in [15] that the stretching effect has to be taken into account to derive accurate models for the modeling of FGM. Thus, these HSDT models have been improved following this recommandation. As previously mentionned, polynomial [16–18], trigonometric [19–23], exponential [24], hyperbolic [25, 26], hybrid [21, 24] functions can be used. For all these models, it should be noted that the number of unknowns remain low (4 in [11, 26, 13], 5 in [7, 19, 8, 23, 24, 18, 25, 12, 9], 6 in [21, 22, 14], 7 for [10]). and most of them are built such that the free boundary conditions on the top and bottom surfaces are fullfiled. Nevertheless, some of them require the determination of parameters involved in the expression of the kinematics, see [22, 26, 12, 9, 14].
This family of models can drive to satisfactory results for monolayered structure with given characteristics, but limitations appear considering multi-layered or sandwich panels. Thus, alternative models have been proposed in literature. The introduction of the so-called Mu-

rakami's zig-zag function in the kinematics as in [17] is a simple way to improve the results. Another way consists in using the Heaviside function [27]. A semi-analytical approach called scaled boundary finite element method (SBFEM) have been also carried out where an analytical formulation can be achieved in the thickness direction [28]. Nevertheless, more accurate theories have been developed based on a LayerWise approach (LW) taking into account the stretching effect [29, 30] or not [31]. Among them, note the extensive works based on the systematic approach developed by Carrera E. with his Carrera's Unified Formulation (CUF) and its extension to FGM material in [30]. Displacement-based and Reissner's Mixed Variational Theorem (RMVT) approaches are addressed in [32, 15]. Discrete layers have been also considered in [33].
Only partial studies on the modeling of FGM plate structures have been mentionned herein and interested readers can refer to the reviews provided in [34–39] where analytical and numerical approaches are identified.

Since few years, some methods based on the separation of variables have shown interesting features to model composite structures and also to reduce computational cost in a reduced-order model (ROM) framework where many analyses have to be performed. For FGM material, the extended Kantorovich method has been applied in [40]. Another interesting way is based on the so-called Proper Generalized Decomposition (PGD). It has been successfully developed for the modeling of laminated / sandwich / FGM structures in [41–45]. In the present work, it is proposed to build an explicit solution of the index law involved in the FGM material properties. This numerical tool based on the ROM allows us to compute very quickly numerous solutions for a wide variety of FGM material avoiding new computations for a new value of the law parameter. In this purpose, the displacements are written under the form of a sum of products of bidimensional functions of (x,y), unidimensional functions of z and also unidimensional functions of the FGM law index. A piecewise fourth-order Lagrange polynomial of z is chosen and a 2D eight-node quadrilateral FE is employed for the in-plane coordinates. Each unknown function of (x,y) is classically approximated using one degree of freedom (dof) per node of the mesh and the LW unknown

functions of z are global for the whole plate. Finally, the deduced non-linear problem implies the resolution of three problems alternatively (one 2D and two 1D problems), in which the number of unknowns is smaller than a classical Layerwise approach.

Hereafter, we present firstly the governing equations and the particular formulation associated to the parametrized FGM plate problem. The assumption on the displacements are given and the derived non-linear problem to be solved is shown. A FE discretization is introduced. Finally, numerical examples are adressed to assess the present method. Configurations involving one-layered and sandwich structures are considered with different FGM laws. The influence of the slenderness ratio is also studied. Our approach is compared to reference solutions and also models available in literature. As our approach provides an explicit solution with respect to a parameter law, the assessment will be performed for some fixed values of the FGM law index.

2. Reference problem description: the governing equations

A composite plate structure occupying the domain $\mathcal{V} = \Omega \times \Omega_z$ is considered. Ω and Ω_z can be defined as $\Omega = [0, a] \times [0, b]$ (a, b being the dimensions of the plate) and $\Omega_z = [-\frac{h}{2}, \frac{h}{2}]$ in a Cartesian coordinate (x, y, z). The thickness of the plate will be denoted h, see Fig. 1.

[Figure 1 about here.]

2.1. Constitutive relation

The plate is constituted of a FGM for which the variations of the characteristics along the thickness are continuous. In the present work, the FGM layers can be single or be a part of a sandwich. Exponential and polynomial functions will be considered and they are applied to either engineering constants (Young Modulus, shear Modulus, Poisson ratio) or directly to material stiffnesses C_{ij}.

Thus, the plate can be made of NC perfectly bonded classical/FGM layers. The constitutive equations for a layer k can be written as

$$\boldsymbol{\sigma}^{(k)} = \mathbf{C}^{(k)}(z)\boldsymbol{\varepsilon}, \quad z\epsilon\Omega_z^k \tag{1}$$

where we denote the stress vector by $\boldsymbol{\sigma}$, the strain vector via $\boldsymbol{\varepsilon}$ and $\Omega_z = \cup_{k=1}^{NC}\Omega_z^k$.

We have

$$\mathbf{C}^{(k)}(z) = \begin{bmatrix} C_{11}^{(k)} & C_{12}^{(k)} & C_{13}^{(k)} & 0 & 0 & C_{16}^{(k)} \\ & C_{22}^{(k)} & C_{23}^{(k)} & 0 & 0 & C_{26}^{(k)} \\ & & C_{33}^{(k)} & 0 & 0 & C_{36}^{(k)} \\ & & & C_{44}^{(k)} & C_{45}^{(k)} & 0 \\ & sym & & & C_{55}^{(k)} & 0 \\ & & & & & C_{66}^{(k)} \end{bmatrix} \tag{2}$$

where $C_{ij}^{(k)}$ are the three-dimensional stiffness coefficients of the layer (k).

Hereafter, it can be assumed that we can write the constitutive law as following without loss of generality:

$$\mathbf{C}^{(k)}(z) = g^{(k)}(z)\ \mathbf{C}_0^{(k)} \tag{3}$$

where $\mathbf{C}_0^{(k)}$ is constant in each layer.

Two cases will be analysed considering polynomial and exponential law, and the Young Modulus is expressed as

$$\begin{aligned} &\text{polynomial:} \quad E(z) = \beta(z,k) = E_b + (E_t - E_b)\left(\tfrac{2z+h}{2h}\right)^k \\ &\text{exponential:} \quad E(z) = \beta(z,k_{exp}) = E_t \exp\left(\gamma\left(\frac{z}{h} - \frac{1}{2}\right)\right) \\ &\qquad\qquad \text{with } \gamma = -\ln\left(\tfrac{E_b}{E_t}\right) = \ln\left(k_{exp}\right) \end{aligned} \tag{4}$$

where k is the volume fraction exponent ($k > 0$), the subscripts t and b stand for the properties of top and bottom of the Layer, respectively, and $k_{exp} = E_t/E_b$ ($E_b = E(-h/2)$ and $E_t = E(h/2)$). These two material indexes allow us to change the behavior of the structure. Note that the Poisson ratio remains constant. The variation of the Young modulus is illustrated in Fig. 2 for various values of k and k_{exp}.

[Figure 2 about here.]

2.2. The classical weak form of the boundary value problem

The plate is only submitted to a surface force $\mathbf{t}$ on $\Gamma_N = \partial\mathcal{V}_{F_{xy}} \times \{z_F\}$ and a prescribed displacement $\mathbf{u} = 0$ on Γ_D. Thus, the classical static problem to be solved can be formulated above.

For admissible displacement $\delta\mathbf{u} \in \delta U$, the variational principle is given by:

find $\mathbf{u} \in U$ such that

$$-\int_{\mathcal{V}} \boldsymbol{\varepsilon}(\delta\mathbf{u})^T \boldsymbol{\sigma}\, d\mathcal{V} + \int_{\Gamma_N} \delta\mathbf{u}^T \mathbf{t}\, d\partial\mathcal{V} = 0, \qquad \forall \delta\mathbf{u} \in \delta U \tag{5}$$

where U is the space of admissible displacements, i.e. $U = \{\mathbf{u} \in (H^1(\mathcal{V}))^3 / \mathbf{u} = \mathbf{0} \text{ on } \Gamma_D\}$ and $\delta U = \{\mathbf{u} \in (H^1(\mathcal{V}))^3 / \mathbf{u} = 0 \text{ on } \Gamma_D\}$.

3. Formulation and resolution of the parametrized FGM plate problem

In this section, the parametrized solution is introduced through a separated variables representation applied to FGM plates. In this way, the displacements are explicitly expressed with respect to both the three classical spatial coordinates (x, y, z), but also one material index k_{FGM} related to the FGM bounded in an interval $\mathcal{I}_{FGM} = [k_{FGM}^{min}, k_{FGM}^{max}]$. Thus, the formulation of this new parametrized problem is given. We will see that a Singular Value Decomposition (SVD) will be required to keep the separability feature of the deduced expressions. The resolution strategy is also explained as the problem to be solved becomes non-linear.

This study is an extension of a previous work on FGM structures [45].

3.1. The displacement and the strain field

As previously stated, we assume that the displacement solution depends on x, y, z, k_{FGM} and is denoted $\mathbf{u}(x, y, z, k_{FGM})$. Thus, in the framework of the PGD, it is expressed as the sum of N products of separated functions ($N \in \mathbb{N}^+$ is the order of the representation).

$$\mathbf{u}(x,y,z,k_{FGM}) \;=\; \sum_{i=1}^{N} g^i_{FGM}(k_{FGM})\mathbf{f}^i(z)\circ\mathbf{v}^i(x,y) \tag{6}$$

where $\mathbf{f^i}(z)$, $\mathbf{v}^i(x,y)$ and $g^i_{FGM}(k_{FGM})$ are unknown functions which must be computed during the resolution process. $\mathbf{f^i}(z)$, $\mathbf{v}^i(x,y)$ and $g^i_{FGM}(k_{FGM})$ are defined on Ω_z, Ω and $\mathcal{I}_{FGM}$, respectively. The "$\circ$" operator in Eq. (6) is Hadamard's element-wise product. We have:

$$\mathbf{f}^i\circ\mathbf{v}^i=\mathbf{v}^i\circ\mathbf{f}^i=\begin{bmatrix} f^i_1(z)v^i_1(x,y)\\ f^i_2(z)v^i_2(x,y)\\ f^i_3(z)v^i_3(x,y)\end{bmatrix} \text{ with } \mathbf{v}^i=\begin{bmatrix} v^i_1(x,y)\\ v^i_2(x,y)\\ v^i_3(x,y)\end{bmatrix}\ \mathbf{f}^i=\begin{bmatrix} f^i_1(z)\\ f^i_2(z)\\ f^i_3(z)\end{bmatrix} \tag{7}$$

Note that the spatial coordinates are splitted into a in-plane / out-of-plane part as it has been already carried out with success in [42, 43] for composite structures. Moreover, only one function with respect to the material parameter k_{FGM} is used.

The strain can be expressed with respect to the reference frame in which the dependance with respect to the space coordinates is omitted:

$$\boldsymbol{\varepsilon}(u)=\sum_{i=1}^{N} g^i_{FGM}(k_{FGM})\begin{bmatrix} f^i_1\,v^i_{1,1}\\ f^i_2\,v^i_{2,2}\\ (f^i_3)'\,v^i_3\\ (f^i_2)'\,v^i_2+f^i_3\,v^i_{3,2}\\ (f^i_1)'\,v^i_1+f^i_3\,v^i_{3,1}\\ f^i_1\,v^i_{1,2}+f^i_2\,v^i_{2,1}\end{bmatrix} \tag{8}$$

where the prime stands for the classical derivative ($f_i'=\dfrac{df_i}{dx}$), and $()_{,\alpha}$ for the partial derivative.

3.2. Formulation of the parametrized problem to be solved

The problem defined by Eq. (5) is considered as a parametrized problem where the material parameter k_{FGM} belongs to the domain $\mathcal{I}_{FGM}$.Thus, the new formulation of this

problem can be given as follows:

find $\mathbf{u} \in \mathcal{U}^{ext}$ ($U^{ext} = \{\mathbf{u} \in (H^1(\mathcal{V} \times \mathcal{I}_{FGM}))^3 / \mathbf{u} = \mathbf{u}_d \text{ on } \Gamma_D \times \mathcal{I}_{FGM}\}$) such that

$$a(\mathbf{u}, \delta\mathbf{u}) = b(\delta\mathbf{u}) \; \forall \delta\mathbf{u} \in \delta\mathcal{U}^{ext} \tag{9}$$

with

$$\begin{aligned} a(\mathbf{u}, \delta\mathbf{u}) &= \int_{\Omega \times \Omega_z \times \mathcal{I}_{FGM}} \boldsymbol{\varepsilon}(\delta\mathbf{u})^T \mathbf{C} \boldsymbol{\varepsilon}(\mathbf{u}) \, d\Omega \, d\Omega_z \, dk_{FGM} \\ b(\delta\mathbf{u}) &= \int_{\Gamma_N \times \mathcal{I}_{FGM}} \delta\mathbf{u}^T \mathbf{t} \, d\Gamma \, dk_{FGM} \end{aligned} \tag{10}$$

3.3. Resolution of the parametrized problem

The expression of the strain, Eq. (8), introduced in the problem in Eq. (9) yields a non-linear parametrized problem that is solved by an iterative process.

First, we assume that the first m ($m < N$) functions $g^i_{FGM}(k_{FGM}), \mathbf{f^i}(z), \mathbf{v}^i(x, y), i = 1, ..., m$ have been already computed. Therefore, the trial function for the iteration $m + 1$ can be written as

$$\mathbf{u}^{m+1}(x, y, z, k_{FGM}) = \mathbf{u}^m(x, y, z, k_{FGM}) + g_{FGM}(k_{FGM}) \mathbf{f}(z) \circ \mathbf{v}(x, y) \tag{11}$$

$$= \sum_{i=1}^{m} g^i_{FGM}(k_{FGM}) \mathbf{f^i}(z) \circ \mathbf{v}^i(x, y) + g_{FGM}(k_{FGM}) \mathbf{f}(z) \circ \mathbf{v}(x, y) \tag{12}$$

where g_{FGM}, $\mathbf{f}$ and $\mathbf{v}$ are the functions to be computed, and $\mathbf{u}^m$ is the associated known sets at iteration m.

Thus, we have to solve the following deduced problem from Eq. (9):

$$a(g_{FGM} \, \mathbf{f} \circ \mathbf{v}, \delta\mathbf{u}) = b(\delta\mathbf{u}) - a(\mathbf{u}^m, \delta\mathbf{u}) \tag{13}$$

The test function becomes

$$\delta(g_{FGM} \, \mathbf{f} \circ \mathbf{v}) = \delta g_{FGM} \, \mathbf{f} \circ \mathbf{v} + g_{FGM} \, \delta\mathbf{f} \circ \mathbf{v} + g_{FGM} \, \mathbf{f} \circ \delta\mathbf{v} \tag{14}$$

Introducing the test function defined by Eq. (14) and the trial function defined by Eq. (12) into the weak form Eq. (13), the three following equations can be obtained:

- for the test function δg_{FGM},

$$a(\mathbf{f} \circ \mathbf{v}\ g_{FGM}, \mathbf{f} \circ \mathbf{v}\ \delta g_{FGM}) \quad = \quad b(\mathbf{f} \circ \mathbf{v}\ \delta g_{FGM}) - a(\mathbf{u}^m, \mathbf{f} \circ \mathbf{v}\ \delta g_{FGM}) \quad \forall \delta g_{FGM} \tag{15}$$

- for the test function $\delta \mathbf{f}$

$$a(g_{FGM}\ \mathbf{v} \circ \mathbf{f}, g_{FGM}\ \mathbf{v} \circ \delta \mathbf{f}) = b(g_{FGM}\ \mathbf{v} \circ \delta \mathbf{f}) - a(\mathbf{u}^m, g_{FGM}\ \mathbf{v} \circ \delta \mathbf{f}) \quad \forall \delta \mathbf{f} \tag{16}$$

- for the test function $\delta \mathbf{v}$

$$a(g_{FGM}\ \mathbf{f} \circ \mathbf{v}, g_{FGM}\ \mathbf{f} \circ \delta \mathbf{v}) = b(g_{FGM}\ \mathbf{f} \circ \delta \mathbf{v}) - a(\mathbf{u}^m, g_{FGM}\ \mathbf{f} \circ \delta \mathbf{v}) \quad \forall \delta \mathbf{v} \tag{17}$$

At this stage, a coupled non-linear problem (Eq. (15), Eq. (16) and Eq. (17)) has to be solved. A fixed point method is used in the present study.

The functions $(\tilde{g}^{(0)}_{FGM}, \tilde{\mathbf{f}}^{(0)}, \tilde{\mathbf{v}}^{(0)})$ are first initialized. Then, a sequence $(\tilde{g}^{(l)}_{FGM}, \tilde{\mathbf{f}}^{(l)}, \tilde{\mathbf{v}}^{(l)})$ satisfying Eq. (15), Eq. (16) and Eq. (17) respectively, is built. For each problem, only one unknown 1D or 2D function has to be found, the two other ones are assumed to be known. This process is summarized in Algorithm 1. The fixed point algorithm is stopped when the distance between two consecutive terms are sufficiently small (Cf. [44]).

3.4. Finite element discretization

The resolution of the present problem is based on a classical finite element approximation. For an element e of the mesh in Ω and Ω_z, the displacement and strain fields associated to $\mathbf{v}, \mathbf{f}$, denoted $\mathbf{v}_e, \mathbf{f}_e$, respectively, are determined from the values of the elementary vector of degrees of freedom (dof) of $\mathbf{q}^v_e$ and $\mathbf{q}^f_e$ by

$$\begin{aligned} \mathbf{v}_e &= \mathbf{N}_{xy}\mathbf{q}^v_e, \quad & \mathcal{E}^e_v &= \mathbf{B}_{xy}\mathbf{q}^v_e, \\ \mathbf{f}_e &= \mathbf{N}_z\mathbf{q}^f_e\ , \quad & \mathcal{E}^e_f &= \mathbf{B}_z\mathbf{q}^f_e \end{aligned} \tag{18}$$

where

$$\mathcal{E}^{eT}_v = \left[\begin{array}{cccccccccc} v_1 & v_{1,1} & v_{1,2} & v_2 & v_{2,1} & v_{2,2} & v_3 & v_{3,1} & v_{3,2} \end{array} \right]$$
$$\mathcal{E}^{eT}_f = \left[\begin{array}{cccccc} f_1 & f'_1 & f_2 & f'_2 & f_3 & f'_3 \end{array} \right]$$

The matrices $\mathbf{N}_{xy}$, $\mathbf{B}_{xy}$, $\mathbf{N}_z$, $\mathbf{B}_z$ contain the interpolation functions, their derivatives and the jacobian components.

Algorithm 1

for $m = 1$ to N_{max} **do**

Initialize $\tilde{g}_{FGM}^{(0)}, \tilde{\mathbf{f}}^{(0)}, \tilde{\mathbf{v}}^{(0)}$

for $l = 1$ to l_{max} **do**

Compute $\tilde{g}_{FGM}^{(l)}$ from Eq. (15), $\tilde{\mathbf{f}}^{(l-1)}, \tilde{\mathbf{v}}^{(l-1)}$ being known

Compute $\tilde{\mathbf{f}}^{(l)}$ from Eq. (16) (linear equation on Ω_z), $\tilde{g}_{FGM}^{(l)}, \tilde{\mathbf{v}}^{(l-1)}$ being known

Compute $\tilde{\mathbf{v}}^{(l)}$ from Eq. (17) (linear equation on Ω), $\tilde{g}_{FGM}^{(l)}, \tilde{\mathbf{f}}^{(l)}$ being known

Check for convergence

end for

Set $g_{FGM}^{m+1} = \tilde{g}_{FGM}^{(l)}$, $\mathbf{f}^{m+1} = \tilde{\mathbf{f}}^{(l)}$, $\mathbf{v}^{m+1} = \tilde{\mathbf{v}}^{(l)}$

Set $\mathbf{u}^{m+1} = \mathbf{u}^m + g_{FGM}^{m+1}\, \mathbf{f}^{m+1} \circ \mathbf{v}^{m+1}$

Check for convergence

end for

3.5. Finite element problem to be solved on Ω

For the sake of simplicity, the upperscript $^{(l)}$ is omitted for the known functions $\tilde{\mathbf{f}}^{(l)}$, $\tilde{g}_{FGM}^{(l)}$ and the functions to be computed $\tilde{\mathbf{v}}^{(l)}$. They are denoted $\tilde{\mathbf{f}}$, $\tilde{g}_{FGM}$ and $\mathbf{v}$, respectively. The following notations are also introduced in Eq. (17):

$$\boldsymbol{\varepsilon}(\tilde{f} \circ v) = \boldsymbol{\Sigma}_{\mathbf{z}}(\tilde{f})\mathcal{E}_{\mathbf{v}} \tag{19}$$

with

$$\boldsymbol{\Sigma}_{\mathbf{z}}(\tilde{f}) = \begin{bmatrix} 0 & \tilde{f}_1 & 0 & 0 & 0 & 0 & 0 & 0 & 0 \\ 0 & 0 & 0 & 0 & 0 & \tilde{f}_2 & 0 & 0 & 0 \\ 0 & 0 & 0 & 0 & 0 & 0 & \tilde{f}_3' & 0 & 0 \\ 0 & 0 & 0 & \tilde{f}_2' & 0 & 0 & 0 & 0 & \tilde{f}_3 \\ \tilde{f}_1' & 0 & 0 & 0 & 0 & 0 & 0 & \tilde{f}_3 & 0 \\ 0 & 0 & \tilde{f}_1 & 0 & \tilde{f}_2 & 0 & 0 & 0 & 0 \end{bmatrix} \tag{20}$$

and $\mathbf{u} = \tilde{g}_{FGM}\mathbf{D}_{\mathbf{z}}(\tilde{f})\mathbf{v} = \tilde{g}_{FGM} \begin{bmatrix} \tilde{f}_1 & 0 & 0 \\ 0 & \tilde{f}_2 & 0 \\ 0 & 0 & \tilde{f}_3 \end{bmatrix} \mathbf{v}$

First of all, it is needed to perform a variable separation for $\beta(z,k)$ from Eq. (4) to keep the separabilty feature of the integrals involved in Eq. (17). For that, a Singular Value Decomposition (SVD) is carried out, and we can obtain the following reduced basis:

$$\beta(z,k_{FGM}) = \sum_{i=1}^{N_{SVD}} \beta_i^z(z)\beta_i^K(k_{FGM}) \tag{21}$$

The effect of the truncated SVD will be discussed in Section 4.1.1. Note that this process is performed only once.

In our framework, the variational problem defined on Ω from Eq. (17) is

$$\int_\Omega \delta\mathcal{E}_\mathbf{v}{}^T \mathbf{k}_{kz}(\tilde{g}_{FGM},\tilde{f})\mathcal{E}_\mathbf{v} d\Omega = \int_{\partial\mathcal{V}_{F_{xy}}} \delta\mathbf{v}^T \mathbf{F}_{kz}(\tilde{g}_{FGM},\tilde{f})\, d\partial\mathcal{V} - \int_\Omega \delta\mathcal{E}_\mathbf{v}{}^T \sigma_\mathbf{kz}(\tilde{g}_{FGM},\tilde{f},u^m) d\Omega \tag{22}$$

where

$$\begin{aligned}
\mathbf{k}_{kz}(\tilde{g}_{FGM},\tilde{f}) &= \sum_{i=1}^{N_{SVD}} \int_{\mathcal{I}_{FGM}} \tilde{g}_{FGM}^2 \beta_i^K\, dk_{FGM} \sum_{p=1}^{NC} \int_{\Omega_z^p} \beta_i^{z(p)}(z)\; \mathbf{\Sigma}_\mathbf{z}(\tilde{f})^T \mathbf{C}_0^{(p)} \mathbf{\Sigma}_\mathbf{z}(\tilde{f}) dz \\
\sigma_\mathbf{kz}(\tilde{g}_{FGM},\tilde{f},u^m) &= \int_{\mathcal{I}_{FGM}} \tilde{g}_{FGM} \sum_{p=1}^{NC} \int_{\Omega_z^p} \beta(z,k_{FGM}) \mathbf{\Sigma}_\mathbf{z}(\tilde{f})^T \mathbf{C}_0^{(p)} \boldsymbol{\varepsilon}(u^m) dz dk_{FGM} \\
\mathbf{F}_{kz}(\tilde{g}_{FGM},\tilde{f}) &= \int_{\mathcal{I}_{FGM}} \tilde{g}_{FGM} dk_{FGM}\; \mathbf{D}_\mathbf{z}(\tilde{f})^T \mathbf{t}\Big|_{z=z_F}
\end{aligned} \tag{23}$$

The upperscript $^{(p)}$ refers to the layer p. Note that the integrals over $\mathcal{I}_{FGM}$ and Ω_z^p in the expressions of $\sigma_\mathbf{kz}$ and $\mathbf{F}_{kz}$ in Eq. (23) are computed in a separated way by introducing the truncated SVD of $\beta(z,k_{FGM})$ given in Eq. (21). The expressions are not shown for brevity reason.

The introduction of the finite element approximation Eq. (18) in the variational Eq. (22) leads to the linear problem:

$$\mathbf{K}_{kz}(\tilde{g}_{FGM},\tilde{f})\,\mathbf{q}^v = \mathbf{R}_{\mathbf{v}kz}(\tilde{g}_{FGM},\tilde{f},u^m) \tag{24}$$

where

- $\mathbf{q}^v$ is the vector of the nodal displacements, associated with the finite element mesh in Ω,

- $\mathbf{K}_{kz}(\tilde{g}_{FGM}, \tilde{f})$ is the mechanical stiffness matrix obtained by summing the elements' stiffness matrices $\mathbf{K}^e_{kz}(\tilde{g}_{FGM}, \tilde{f}) = \int_{\Omega_e} \left[\mathbf{B}^T_{xy}\mathbf{k}_{kz}(\tilde{g}_{FGM}, \tilde{f})\mathbf{B}_{xy}\right] d\Omega_e$

- $\mathbf{R}_{\mathbf{v}kz}(\tilde{g}_{FGM}, \tilde{f}, u^m)$ is the equilibrium residual obtained by summing the elements' residual load vectors:
$\mathbf{R}^{\mathbf{e}}_{\mathbf{v}kz}(\tilde{g}_{FGM}, \tilde{f}, u^m) = \int_{\partial\mathcal{V}^e_{F_{xy}}} \mathbf{N}^T_{xy}\mathbf{F}_{kz}(\tilde{g}_{FGM}, \tilde{f}) d\partial\mathcal{V}_e - \int_{\Omega_e} \mathbf{B}^T_{xy}\sigma_{\mathbf{kz}}(\tilde{g}_{FGM}, \tilde{f}, u^m) d\Omega_e$

3.6. Finite element problem to be solved on Ω_z

As previously, the known functions $\tilde{\mathbf{v}}^{(l-1)}$ and $\tilde{g}^{(l)}_{FGM}$ will be denoted $\tilde{\mathbf{v}}$ and $\tilde{g}_{FGM}$, respectively and the functions $\tilde{\mathbf{f}}^{(l)}$ to be computed will be denoted $\mathbf{f}$. The strain included in Eq. (16) is defined as

$$\boldsymbol{\varepsilon}(\tilde{v} \circ f) = \boldsymbol{\Sigma}_{\mathbf{xy}}(\tilde{v})\mathcal{E}_{\mathbf{f}} \tag{25}$$

where

$$\boldsymbol{\Sigma}_{\mathbf{xy}}(\tilde{v}) = \begin{bmatrix} \tilde{v}_{1,1} & 0 & 0 & 0 & 0 & 0 \\ 0 & 0 & \tilde{v}_{2,2} & 0 & 0 & 0 \\ 0 & 0 & 0 & 0 & 0 & \tilde{v}_3 \\ 0 & 0 & 0 & \tilde{v}_2 & \tilde{v}_{3,2} & 0 \\ 0 & \tilde{v}_1 & 0 & 0 & \tilde{v}_{3,1} & 0 \\ \tilde{v}_{1,2} & 0 & \tilde{v}_{2,1} & 0 & 0 & 0 \end{bmatrix} \tag{26}$$

and the displacement is $\mathbf{u} = \tilde{g}_{FGM}\mathbf{D}_{\mathbf{xy}}(\tilde{v})\mathcal{E}_{\mathbf{f}} = \tilde{g}_{FGM} \begin{bmatrix} \tilde{v}_1 & 0 & 0 & 0 & 0 & 0 \\ 0 & 0 & 0 & 0 & 0 & 0 \\ 0 & 0 & \tilde{v}_2 & 0 & 0 & 0 \\ 0 & 0 & 0 & 0 & 0 & 0 \\ 0 & 0 & 0 & 0 & \tilde{v}_3 & 0 \\ 0 & 0 & 0 & 0 & 0 & 0 \end{bmatrix} \mathcal{E}_{\mathbf{f}}$

The variational problem defined on Ω_z from Eq. (16) is

$$\sum_{p=1}^{NC} \int_{\Omega_z^p} \delta\mathcal{E}_{\mathbf{f}}{}^T \left[\sum_{i=1}^{N_{SVD}} k_k^i(\tilde{g}_{FGM}) \beta_i^z(z) \right] \mathbf{k}_{xy}^{(p)}(\tilde{v}) \mathcal{E}_{\mathbf{f}} dz = \delta\mathcal{E}_{\mathbf{f}}{}^T\big|_{z=z_F} \mathbf{F}_{xy}(\tilde{g}_{FGM}, \tilde{v}) - \sum_{p=1}^{NC} \int_{\Omega_z^p} \delta\mathcal{E}_{\mathbf{f}}{}^T \sigma_{\mathbf{kxy}}{}^{(p)}(\tilde{g}_{FGM}, \tilde{v}, u^m) dz \tag{27}$$

where $k_k^i(\tilde{g}_{FGM})$, $\mathbf{k}_{xy}^{(p)}(\tilde{v})$, $\sigma_{\mathbf{kxy}}{}^{(p)}(\tilde{g}_{FGM}, \tilde{v}, u^m)$ and $\mathbf{F}_{xy}(\tilde{g}_{FGM}, \tilde{v})$ can be expressed under the following separated form:

$$\begin{aligned}
&k_k^i(\tilde{g}_{FGM}) = \int_{\mathcal{I}_{FGM}} \tilde{g}_{FGM}^2 \beta_i^K \, dk_{FGM} \\
&\mathbf{k}_{xy}^{(p)}(\tilde{v}) = \int_{\Omega} \mathbf{\Sigma_{xy}}(\tilde{v})^T \mathbf{C}_0^{(p)} \mathbf{\Sigma_{xy}}(\tilde{v}) d\Omega \\
&\sigma_{\mathbf{kxy}}{}^{(p)}(\tilde{g}_{FGM}, \tilde{v}, u^m) = \int_{\mathcal{I}_{FGM}} \int_{\Omega} \tilde{g}_{FGM} \, \beta(z, k_{FGM}) \mathbf{\Sigma_{xy}}(\tilde{v})^T \mathbf{C}_0^{(p)} \boldsymbol{\varepsilon}(u^m) d\Omega dk_{FGM} \\
&\mathbf{F}_{xy}(\tilde{g}_{FGM}, \tilde{v}) = \int_{\mathcal{I}_{FGM}} \tilde{g}_{FGM} dk_{FGM} \int_{\partial\mathcal{V}_{F_{xy}}} \mathbf{D_{xy}}(\tilde{v})^T \mathbf{t} \, d\partial\mathcal{V}_{xy}
\end{aligned} \tag{28}$$

Note that the expression of $\sigma_{\mathbf{kxy}}{}^{(p)}(\tilde{g}_{FGM}, \tilde{v}, u^m)$ involves two separated integrals over $\mathcal{I}_{FGM}$ and Ω by introducing the SVD of the term $\beta(z, k_{FGM})$. It is not detailed for conciseness reason.

The introduction of the finite element discretization Eq. (18) in the variational Eq. (27) leads to the linear problem:

$$\mathbf{K}_{kxy}(\tilde{g}_{FGM}, \tilde{v}) \, \mathbf{q}^f = \mathcal{R}_f(\tilde{g}_{FGM}, \tilde{v}, u^m) \tag{29}$$

where

- $\mathbf{q}^f$ is the vector of degree of freedom associated with the F.E. approximations in Ω_z.
- $\mathbf{K}_{kxy}(\tilde{g}_{FGM}, \tilde{v})$ is obtained by summing the elements' stiffness matrices:

$$\mathbf{K}_{kxy}{}^e(\tilde{g}_{FGM}, \tilde{v}) = \int_{\Omega_{ze}^p} \left[\sum_{i=1}^{N_{SVD}} k_k^i(\tilde{g}_{FGM}) \beta_i^z(z) \right] \left[\mathbf{B}_z^T \mathbf{k}_{xy}^{(p)}(\tilde{v}) \mathbf{B}_z \right] dz_e \tag{30}$$

- $\mathcal{R}_f(\tilde{g}_{FGM}, \tilde{v}, u^m)$ is obtained by summing the residual' vectors:

$$\mathcal{R}_f^e(\tilde{g}_{FGM}, \tilde{v}, u^m) = \mathbf{B}_z^T|_{z=z_F} \mathbf{F}_{xy}(\tilde{g}_{FGM}, \tilde{v}) - \int_{\Omega_{ze}^p} \left[\mathbf{B}_z^T {\sigma_{\mathbf{kxy}}}^{(p)}(\tilde{g}_{FGM}, \tilde{v}, u^m) \right] dz_e \quad (31)$$

3.7. Problem to be solved on $\mathcal{I}_{FGM}$

In this part, we will focus on the computation of the unknown function $\tilde{g}_{FGM}^{(l)}$, denoted g_{FGM}, the other ones $\tilde{\mathbf{v}}^{(l-1)}$ and $\tilde{\mathbf{f}}^{(l-1)}$ being known. They are denoted $\tilde{\mathbf{v}}$ and $\tilde{\mathbf{f}}$ respectively. The problem Eq. (15) can be solved in a straightforward manner following:

$$g_{FGM}(k_{FGM}) = \frac{\displaystyle\int_{\partial \mathcal{V}_{F_{xy}}} \tilde{\mathbf{v}}^T \mathbf{F}_z(\tilde{f})\, d\partial\mathcal{V} - \sum_{i=1}^{N_{SVD}} \beta_i^K(k_{FGM}) \sigma_{\mathbf{xyz}}^{\mathbf{i}}(\tilde{f}, \tilde{v}, u^m) d\Omega}{\displaystyle\sum_{i=1}^{N_{SVD}} k_{xyz}^i(\tilde{f}, \tilde{v}) \beta_i^K(k_{FGM})} \quad (32)$$

where

$$\begin{aligned} k_{xyz}^i(\tilde{f}, \tilde{v}) &= \int_\Omega {\tilde{\mathcal{E}}_{\mathbf{v}}}^T \mathbf{k}_z^i(\tilde{f}) \tilde{\mathcal{E}}_{\mathbf{v}} d\Omega \text{ with } \mathbf{k}_z^i(\tilde{f}) = \sum_{p=1}^{NC} \int_{\Omega_z^p} \beta_i^z(z) \mathbf{\Sigma_z}(\tilde{f})^T \mathbf{C}_0^{(p)} \mathbf{\Sigma_z}(\tilde{f}) dz \\ \sigma_{\mathbf{xyz}}^{\mathbf{i}}(\tilde{f}, \tilde{v}, u^m) &= \int_\Omega \sum_{p=1}^{NC} \int_{\Omega_z^p} \beta_i^z(z) {\tilde{\mathcal{E}}_{\mathbf{v}}}^T \mathbf{\Sigma_z}(\tilde{f})^T \mathbf{C}_0^{(p)} \boldsymbol{\varepsilon}(u^m) dz d\Omega \end{aligned} \quad (33)$$

In practice, the function g_{FGM} is computed at the Gauss points coordinate in N_h elements of the domain $\mathcal{I}_{FGM}$.

Remark: The formulation given above is general as it can be applied for any types of material, i.e. FGM or classical layer. The layer p can be isotropic or orthotropic. In this case, we have $\beta_i^K(k_{FGM}) = 1$, $\beta_i^z(z) = 1$ and $N_{SVD} = 1$.

4. Numerical results

In the numerical examples, an eight-node quadrilateral FE based on the classical Serendipity interpolation functions is used for the unknowns depending on the in-plane coordinates.

For the unknowns depending on the z-coordinate, the displacement is described by a fourth-order interpolation as it is justified in [44].

Hereafter, some test cases are addressed to illustrate the behavior of the method and assess its accuracy. A classical numerical example proposed by [19] involving a one-layered plate is first given. A convergence study on the number of the SVD terms used in Eq. (21) and on the number of triplets of this method is carried out. A second part is dedicated to the same test case but with an exponential law instead of a polynomial one for the FGM plate. Various slenderness ratios are considered. In the third example, a sandwich structure with a FGM core is considered.

The present approach, denoted VS-LD4, is compared with both reference solutions and other models available in open literature (see Tab. 1). Unless otherwise mentioned, the fourth-order layerwise model LD4, referring to the systematic work of Carrera ("Carrera's Unified Formulation" (CUF)) will be considered as the reference solution. If the numerical results are not available in the literature, values are provided using a home code implemented by the authors.

It should be noted that many numerical assessments in literature involve a bi-sinusoidal pressure on the structure. For the present work, a uniform distributed pressure will be considered as it can be considered as a more severe and representative case.

[Table 1 about here.]

4.1. one-layered FGM plate with a polynomial law

In this section, a one-layered FGM plate is considered with different slenderness ratios. The data is given as follows:

geometry: square FGM plate with length-to-thickness ratio $S = a/h = 5, 10, 20$

boundary conditions: simply-supported plate subjected to a uniform pressure: $p(x, y) = p_0$

material properties: elastic properties varying along the thickness direction z by a polynomial law, as proposed by Zenkour [19]; The plate is made of aluminum on the bottom and alumina on the top, and the following functional relationship is considered for $E(z)$:

$$E(z) = E_m + (E_c - E_m)\left(\frac{2z+h}{2h}\right)^k$$

where $E_b = E_m = 70$ GPa, $E_t = E_c = 380$ GPa are the elastic modulus of the aluminium and alumina, respectively. k is the volume fraction exponent ($k > 0$). $\nu = 0.3$ is considered as constant.

mesh: $N_x = N_y = 32$ where N_x and N_y are the number of elements along the x and y directions, respectively.

number of dofs: $Ndof_{xy} = 3 * (3.N_x.N_y + 2(N_x + N_y) + 1)$ and $Ndof_z = 12 \times N_z + 3$ are the number of dofs of the two problems associated with v_j^i and f_j^i respectively. N_z is the number of numerical layers. So, the total number of dofs is $Ndof_{xy} + Ndof_z$.

results displacements and stresses are made non-dimensional according to

$$\bar{u}(z) = u_1(0, b/2, z)\ \frac{100\ E_c\ h^3}{p_0\ a^4};\ \bar{w}(z) = u_3(a/2, b/2, z)\ \frac{10\ E_c\ h^3}{p_0\ a^4};$$
$$\bar{\sigma}_{11}(z) = \sigma_{11}(a/2, b/2, z)\ \frac{h}{a\ p_0};\ \bar{\sigma}_{13}(z) = \sigma_{13}(0, b/2, z)\ \frac{h}{a\ p_0}$$

The computations are carried out for $k \in [k_{min} = 1, k_{max} = 10]$ with $N_h = 90$ (defined in Section 3.7). Based on previous results available in [45], eight numerical layers are considered. The results are built with 30 triplets (see Section 4.1.2).

4.1.1. Convergence study: number of SVD terms

Firstly, a convergence study on the number of SVD terms to be built (see Section 3.5) is shown. The reference solution corresponds to the solution without SVD. Based on the error rates provided in Tab. 2 for different values of k, the values of the displacements and stresses are accurate for $N_{SVD} \geq 5$. In the subsequent tests, this value is chosen. Note that the convergence is not strictly monotonous as the indicator is local. Nevertheless, this phenomenon occurs for small values of this indicator.

[Table 2 about here.]

4.1.2. Convergence study: number of triplets

In this section, a convergence study is carried out related to the number of triplets to be built. An error rate is defined as

$$Err_X(n) = 100 \max_k \left(\frac{X^n_{VS-LD4} - X_{ref}}{X_{ref}} \right)$$

where X^n_{VS-LD4} is the solution $(\bar{u}(-h/4),\ \bar{w}(0),\ \bar{\sigma}_{11}(h/2),\ \bar{\sigma}_{13}(0))$ computed with n triplets.

From Fig. 3, we can conclude that the PGD process converges. Considering a yield error rate at 0.5%, it is required to build 25 and 30 triplets for $S = 10$ and $S = 5$, respectively. As classically observed, the convergence rate of the stresses is lower than those of the displacements.

[Figure 3 about here.]

4.1.3. Assessment of the present model

First of all, the variation of the 18 first functions g^i_{FGM} are shown in Fig. 4 to illustrate the method and the explicit expression with respect to the volume fraction exponent k.

[Figure 4 about here.]

Then, the non-dimensional deflection and stresses are given in Tab. 3 for various values of volume fraction exponent k. The use of the LD4 model requires a new computation for each value of k whereas the present approach (VS-LD4 model) provides an explicit solution of k. It can be inferred from this table that the results are in excellent agreement with the reference solution. The maximum error rate is 0.36%.

[Table 3 about here.]

For further assessment, the present approach is compared with models available in literature. The results are summarized in Tab. 4. The main characteristics of these models are recalled in Tab. 1. As it can be expected, the most accurate model involves a LW approach (Nik17) with a maximum difference of 2%. The maximum rate is related to a HSDT model without the stretching effect (Aka15 - $\varepsilon_{zz} = 0$). Nevertheless, the gain with respect to the HSDT model without the stretching effect is not proved for this example. Globally, for these ESL models, the error rate is higher for the transverse shear stress. Finally, we can also notice that the error rate depends on the value of k. So, the accuracy of the models presented in this table is sensitive to this material parameter, what renders them less robust.

[Table 4 about here.]

Fig. 5 and Fig. 6 show the effect of the power-law index k on the in-plane / transverse displacements and in-plane / transverse shear stresses. These figures illustrate the interest of the approach. Results issued from the previous models in Tab. 4 are also reported when available. It can be seen that the results are close for the transverse displacement and the in-plane stress. The main differences occur for the transverse shear stress. It is confirmed that the present approach is in excellent agreement with the reference solution despite the value of k. On the contrary, the accuracy of HSDT models depends on this parameter. The maximum error rate occurs for $k = 4$. From these figures, two different parts can be distinguished on the graphes, namely for $k \leq 4$ and $k \geq 4$. For $k \leq 4$, a high variation of the displacements and stresses occurs. Then, for $k \geq 4$, the in-plane displacement and the transverse shear stress remain nearly constant.

[Figure 5 about here.]

[Figure 6 about here.]

Finally, the distributions of the normal and transverse shear stresses are shown in Fig. 7 and Fig. 8 for different slenderness ratios (same scale used for each graph). The results issued from [19] (only the normal stress) are also given for comparison. It can be emphasized

again the good quality of the present approach when compared to the LD4 model despite the different distributions of stresses. We can also notice that the HSDT model can predict the bending stress with accuracy. As far as the transverse shear stress is concerned, the distribution is asymmetric due to the FGM properties.

[Figure 7 about here.]

[Figure 8 about here.]

4.2. one-layered FGM plate with a exponential law

The same test case as in the previous section (Section 4.1) is addressed, but the material properties are different. They are assumed to vary in the thickness direction according to an exponential law following:

$$\begin{aligned} E(z) &= E_t \exp\left(\gamma\left(\frac{z}{h}-\frac{1}{2}\right)\right) \\ \text{with } \gamma &= -\ln\left(\frac{E_b}{E_t}\right) = \ln\left(k_{exp}\right) \end{aligned} \tag{34}$$

where $E_b = 10^9$ Pa and $E_t = k_{exp}E_b$ are the Young Modulus at the bottom and the top of the plate, respectively. The variation domain of k_{exp} is $[0.1, 10]$. $N_h = 90$.

By referring to the literature, two slenderness ratios are considered, namely $S = 10/3$ and $S = 5$. In our approach, 16 numerical layers are used so that the free boundary conditions on the upper and lower surfaces be fulfilled. 25 and 20 triplets are built for $S = 10/3$ and $S = 5$, respectively.

First, the present model and other models from the literature are compared with the reference one (LD4) in Tab. 5 and Tab. 6. 3D FEM Ansys results are provided in [48] using a $36 \times 36 \times 36$ SOLID 45 brick elements, denoted FEM3D-Vag. In addition, we have carried out a 3D FEM Ansys analysis with a very refined mesh ($60 \times 60 \times 100$ with a refinement near the top/bottom surface), denoted FEM3D. Comparing these two 3D FEM

approaches, it can be concluded that the mesh used for the FEM3D-Vag results does not drive to converged results. In particular, the values of the in-plane stress are very sensitive to the mesh refinement as the material is modelized with a piecewise constant Young Modulus through the thickness. These new 3D FEM results are very close to the LD4 model. Thus, it is justified to use the latter as a reference one.

From Tab. 5 and Tab. 6, it can be also noticed that the accuracy of the VS-LD4 model is excellent. The error rate is less than 1.3% regardless of the $k_{exp} = E_t/E_b$ ratio and the value of S. For the other models, the error rate depends on the ratio parameter. Globally, it seems that it increases with the value of k_{exp} for the in-plane stress. The most severe case corresponds to the value of $k_{exp} = 10$ where all models from literature drives to an error rate of more than 5% for $\bar{w}$ and 8% for $\bar{\sigma}_{11}$. We also observe that the accuracy of these models decreases as the slenderness ratio decreases.

[Table 5 about here.]

[Table 6 about here.]

For further illustrations, the influence of the $k_{exp} = E_t/E_b$ ratio is shown in Fig. 9 and Fig. 10 for the exponentially graded plate. Variations of the displacement and stresses with respect to k_{exp} are shown in Fig. 9 while distributions of the stresses through the thickness is given in Fig. 10 for different values of k_{exp}. The deflection and the bending stress at the bottom of the plate increase as k_{exp} increases. The maximum shear stress curve reaches a minimum value when k_{exp} is about 0.6. The through-thickness distribution of the transverse shear stress has a peak that shifts from the bottom to the top of the plate with the increase of k_{exp}. For $k_{exp} = 1$ corresponding to a homogeneous structure, the maximum is located at the middle surface, but the curve is never symmetric regardless of k_{exp} due to the low slenderness ratio. The FGM behavior can be also seen through the distribution of the in-plane stress $\bar{\sigma}_{11}$ along the thickness as it does not vary linearly excepted for $k_{exp} = 1$. Moreover, Fig. 10 illustrates the good accuracy of the present VS-LD4 model as it has already been seen before.

[Figure 9 about here.]

[Figure 10 about here.]

4.3. Sandwich plate with a FGM core

In this section, a sandwich plate where the FGM properties of the core are those given by Zenkour [19] is considered. The test case comes from [15] and is described as follows:

geometry: square sandwich plate ($a = b = 1$ m) with length-to-thickness ratio $S = 4$, constituted of three layers, the thickness of the faces and the core is $h_f = 0.1h$ and $h_c = 0.8h$, respectively.

boundary conditions: simply-supported plate on all sides subjected to a uniform distributed pressure $p(x, y) = p_0$

material properties: The two external faces are in aluminium at the bottom and in alumina at the top.
bottom face sheets: isotropic material with $E = 70$ GPa, $\nu = 0.3$ (aluminium)
top face sheets: isotropic material with $E = 380$ GPa, $\nu = 0.3$ (alumina)
Core : FGM as in Section 4.1

mesh: $N_x = N_y = 32$

number of dofs: $Ndof_{xy} = 9603$ and $Ndof_z = 12 \times N_z + 3 = 111$

number of dofs for LD4: $N_{LW} = 3.(4.N_z + 1).(3.N_x.N_y + 2(N_x + N_y) + 1) = 355311$

results: non-dimensional results as in Section 4.1

We have $k \in [1, 10]$ and $N_h = 90$. Three numerical layers per physical layer are used. Variations of non-dimensional central deflection w, in-plane displacement, normal and transverse shear stresses as a function of the power-law index k are given in Fig. 11. It can be

inferred from this figure that very accurate results are obtained when compared to the reference model for various fixed values of k. The through-thickness distributions of the stresses shown in Fig. 12 for $k = 1$ and $k = 10$ allows us to make the same remark. We can notice that the peak of $\bar{\sigma}_{13}$ shifts toward the upper surface of the plate when k varies from 1 to 10. Such distributions cannot be obtained by ESL models.

[Figure 11 about here.]

[Figure 12 about here.]

5. Conclusion

In the present work, an approach based on a variable separation is developed to build an explicit solution with respect to the FGM material parameter. In this way, numerous computations for any values of the index parameter are avoided. It can be advantageously used in the framework of iterative process such as optimization or identification problems. The assessment of the approach is performed through the comparison with a quasi-3D model based on a layerwise assumption and 3D FEM analysis with various fixed values of the material parameter. Large variety of models available in literature are also provided. It can be concluded that the accuracy of our model is very good considering various configurations (one-layered or sandwich), FGM laws and slenderness ratios.

References

[1] V. Birman, L. W. Byrd, Modeling and analysis of functionally graded materials and structures., Appl. Mech. Rev. 60 (5) (2007) 195–216.

[2] M. Kashtalyan, Three-dimensional elasticity solution for bending of functionally graded rectangular plates., European J. of Mechanics A. Solids 23 (2004) 853–64.

[3] M. Kashtalyan, M. Menshykova, Three-dimensional elasticity solution for sandwich panels with a functionally graded core., Compos. Struct. 87 (2008) 36–43.

[4] V. Burlayenko, T. Sadowski, Free vibrations and static analysis of functionally graded sandwich plates with three-dimensional finite elements, Meccanica 55 (4) (2020) 815–832.

[5] S.-H. Chi, Y.-L. Chung, Mechanical behavior of functionally graded material plates under transverse load - part i: Analysis., Int. J. Solids Struct. 43 (13) (2006) 3657–3674.

[6] Z. Cheng, R. Batra, Deflection relationships between the homogeneous kirchhoff plate theory and different functionally graded plate theories, Archives of Mechanics 52 (1) (2000) 143–158.

[7] J. Reddy, Analysis of functionally graded plates., Int. J. Num. Meth. Eng. 47 (2000) 663–684.

[8] A. Ferreira, R. Batra, C. Roque, L. Qian, P. Martins, Static analysis of functionally graded plates using third-order shear deformation theory and a meshless method, Compos. Struct. 69 (4) (2005) 449–457.

[9] R. Kumar, A. Lal, B. Singh, J. Singh, New transverse shear deformation theory for bending analysis of FGM plate under patch load., Compos. Struct. 208 (2019) 91–100.

[10] C. H. Thai, A. Ferreira, P. Phung-Van, A nonlocal strain gradient isogeometric model for free vibration and bending analyses of functionally graded plates, Compos. Struct. 251 (2020) 112634. doi:https://doi.org/10.1016/j.compstruct.2020.112634.

[11] H.-T. Thai, T. P. Vo, A new sinusoidal shear deformation theory for bending, buckling, and vibration of functionally graded plates, Appl. Math. Model. 37 (5) (2013) 3269–3281.

[12] V.-H. Nguyen, T.-K. Nguyen, H.-T. Thai, T. Vo, A new inverse trigonometric shear deformation theory for isotropic and functionally graded sandwich plates, Composite Part B : Eng. J. 66 (2014) 233–246.

[13] H. Nguyen-Xuan, L. V. Tran, C. H. Thai, S. Kulasegaram, S. Bordas, Isogeometric analysis of functionally graded plates using a refined plate theory., Composite Part B : Eng. J. 64 (2014) 222–234.

[14] M. Li, C. G. Soares, R. Yan, A novel shear deformation theory for static analysis of functionally graded plates., Compos. Struct. 250 (2020) 112559.

[15] E. Carrera, S. Brischetto, M. Cinefra, M. Soave, Effects of thickness stretching in functionally graded plates and shells., Composite Part B : Eng. J. 42 (2011) –.

[16] L. Qian, R. Batra, L. Chen, Static and dynamic deformations of thick functionally graded elastic plates by using higher-order shear and normal deformable plate theory and meshless local petrov–galerkin method, Composite Part B : Eng. J. 35 (6-8) (2004) 685–697.

[17] S. Natarajan, M. Ganapathi, Bending and vibration of functionally graded material sandwich plates using an accurate theory., Finite Elem. Anal. Des. 57 (2012) 32–42.

[18] H.-T. Thai, D.-H. Choi, Improved refined plate theory accounting for effect of thickness stretching in functionally graded plates, Composite Part B : Eng. J. 56 (2014) 705–716.

[19] A. Zenkour, Generalized shear deformation theory for bending analysis of functionally graded plates., Appl. Math. Model. 30 (2006) 67–84.

[20] A. Neves, A. Ferreira, E. Carrera, C. Roque, M. Cinefra, R. Jorge, C. Soares, A quasi-3d sinusoidal shear deformation theory for the static and free vibration analysis of functionally graded plates., Composite Part B : Eng. J. 43 (2012) 711–725.

[21] J. Mantari, C. G. Soares, Generalized hybrid quasi-3d shear deformation theory for the static analysis of advanced composite plates., Compos. Struct. 94 (8) (2012) 2561–2575.

[22] J. Mantari, C. G. Soares, Optimized sinusoidal higher order shear deformation theory for the analysis of functionally graded plates and shells, Composite Part B : Eng. J. 56 (2014) 126–136.

[23] H.-T. Thai, S.-E. Kim, A simple quasi-3d sinusoidal shear deformation theory for functionally graded plates., Compos. Struct. 99 (2013) 172–180.

[24] J. Mantari, C. G. Soares, Five-unknowns generalized hybrid-type quasi-3d hsdt for advanced composite plates, Appl. Math. Model. 39 (18) (2015) 5598–5615.

[25] Z. Belabed, M. Houari, A. Tounsi, S. Mahmoud, O. Bég, An efficient and simple higher order shear and normal deformation theory for functionally graded material (FGM) plates, Composite Part B : Eng. J. 60 (2014) 274–283.

[26] J. Mantari, C. G. Soares, Four-unknown quasi-3d shear deformation theory for advanced composite plates, Compos. Struct. 109 (2014) 231–239.

[27] A. Garg, H. Chalak, A. Chakrabarti, Bending analysis of functionally graded sandwich plates using hozt including transverse displacement effects, Mechanics Based Design of Structures and Machines (2020) 1–15.

[28] W. Ye, J. Liu, J. Zhang, F. Yang, G. Lin, A new semi-analytical solution of bending, buckling and free vibration of functionally graded plates using scaled boundary finite element method, Thin-Walled Struct. 163 (2021) 107776.

[29] S. Brischetto, R. Leetsch, E. Carrera, T. Wallmersperger, B. Kröplin, Thermo-mechanical bending of functionally graded plates, J. Thermal Stresses 31 (3) (2008) 286–308.

[30] E. Carrera, S. Brischetto, A. Robaldo, Variable kinematic model for the analysis of functionally graded material plates., AIAA J. 46 (2008) 194–203.

[31] H. Hirane, M.-O. Belarbi, M. S. A. Houari, A. Tounsi, On the layerwise finite element formulation for static and free vibration analysis of functionally graded sandwich plates, Engineering with Computers (2021) 1–29.

[32] S. Brischetto, E. Carrera, Advanced mixed theories for bending analysis of functionally graded plates., Comput. Struct. 88 (2010) 1474–1483.

[33] F. Ramirez, P. Heyliger, E. Pan, Static analysis of functionally graded elastic anisotropic plates using a discrete layer approach, Composites Part B: Engineering 37 (1) (2006) 10–20.

[34] D. Jha, T. Kant, R. Singh, A critical review of recent research on functionally graded plates, Compos. Struct. 96 (2013) 833–849. doi:https://doi.org/10.1016/j.compstruct.2012.09.001.

[35] K. Swaminathan, D. Naveenkumar, A. Zenkour, E. Carrera, Stress, vibration and buckling analyses of FGM plates - a state-of-the-art review., Compos. Struct. 120 (2015) 10–31.

[36] A. Gupta, M. Talha, Recent development in modeling and analysis of functionally graded materials and structures., Progress in Aerospace Sciences 79 (2015) 1–14.

[37] H.-T. Thai, S.-E. Kim, A review of theories for the modeling and analysis of functionally graded plates and shells, Compos. Struct. 128 (2015) 70–86.

[38] P. S. Ghatage, V. R. Kar, P. E. Sudhagar, On the numerical modelling and analysis of multi-directional functionally graded composite structures: A review, Compos. Struct. 236 (2020) 111837. doi:https://doi.org/10.1016/j.compstruct.2019.111837.

[39] C.-P. Wu, Y.-C. Liu, A review of semi-analytical numerical methods for laminated composite and multilayered functionally graded elastic/piezoelectric plates and shells, Compos. Struct. 147 (2016) 1–15. doi:https://doi.org/10.1016/j.compstruct.2016.03.031.

[40] M. Aghdam, K. Bigdeli, N. Shahmansouri, A semi-analytical solution for bending of moderately thick doubly curved functionally graded panels, Mech. Advanced Mater. Struct. 17 (5) (2010) 320–327.

[41] M. Savoia, J. Reddy, A variational approach to three-dimensional elasticity solutions of laminated composite plates, J. Applied Mech. ASME 59 (1992) 166–175.

[42] B. Bognet, F. Bordeu, F. Chinesta, A. Leygue, A. Poitou, Advanced simulation of models defined in plate geometries: 3D solutions with 2D computational complexity., Comput. Methods Appl. Mech. Eng. 201-204 (2012) 1–12, doi: 10.1016/j.cma.2011.08.025.

[43] P. Vidal, L. Gallimard, O. Polit, Composite beam finite element based on the proper generalized decomposition., Comput. Struct. 102-103 (2012) 76–86, -doi: 10.1016/j.compstruc.2012.03.008.

[44] P. Vidal, L. Gallimard, O. Polit, Proper generalized decomposition and layer-wise approach for the modeling of composite plate structures., Int. J. Solids Struct. 50 (14-15) (2013) 2239–2250, -doi: 10.1016/j.ijsolstr.2013.03.034.

[45] P. Vidal, L. Gallimard, O. Polit, E. Valot, Analysis of functionally graded plates based on a variable separation method., Mech. Advanced Mater. Struct.-doi:10.1080/15376494.2021.1942597.

[46] S. Nikbakht, S. J. Salami, M. Shakeri, Three dimensional analysis of functionally graded plates up to yielding, using full layer-wise finite element method, Compos. Struct. 182 (2017) 99–115.

[47] S. Akavci, A. Tanrikulu, Static and free vibration analysis of functionally graded plates based on a new quasi-3d and 2d shear deformation theories, Composite Part B : Eng. J. 83 (2015) 203–215.

[48] R. Vaghefi, G. Baradaran, H. Koohkan, Three-dimensional static analysis of thick functionally graded plates by using meshless local petrov–galerkin (mlpg) method, Eng. Anal. Bound. Elem. 34 (6) (2010) 564–573. doi:https://doi.org/10.1016/j.enganabound.2010.01.005.

List of Figures

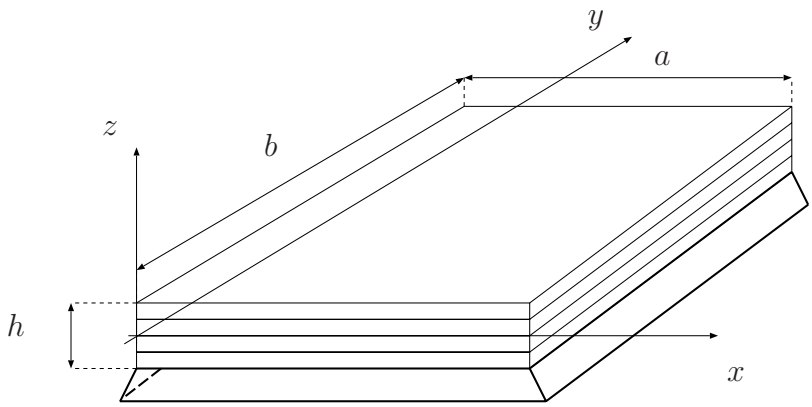

Figure 1: Geometry of the plate

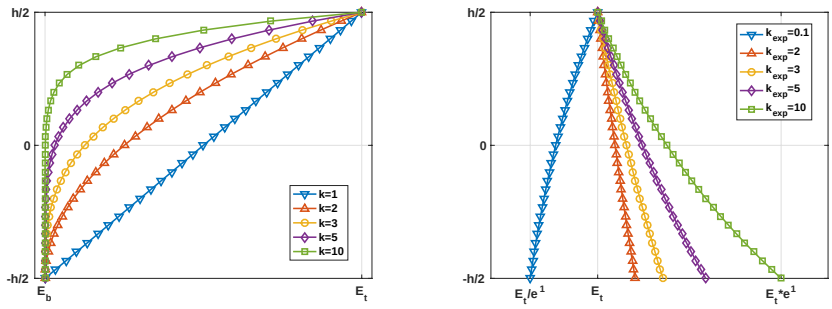

(a) polynomial law (b) exponential law

Figure 2: variation of the Young Modulus along the thickness for various values of k and k_{exp}

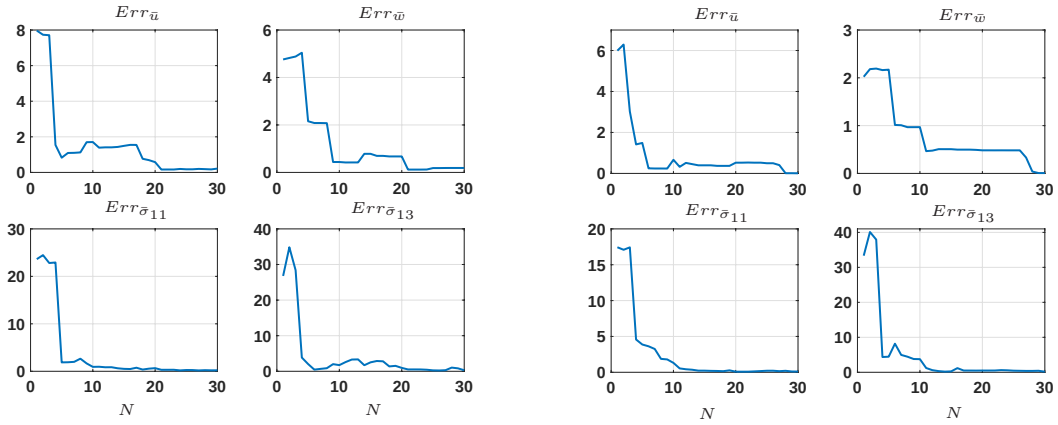

(a) $S = 5$ (b) $S = 10$

Figure 3: Error rate versus the number of triplets - one-layered - polynomial law

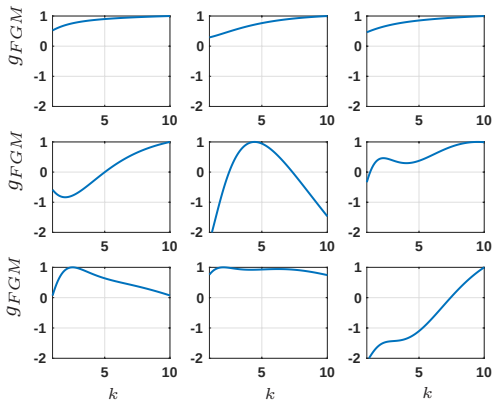

(a) functions g^i_{FGM} - i=1-9

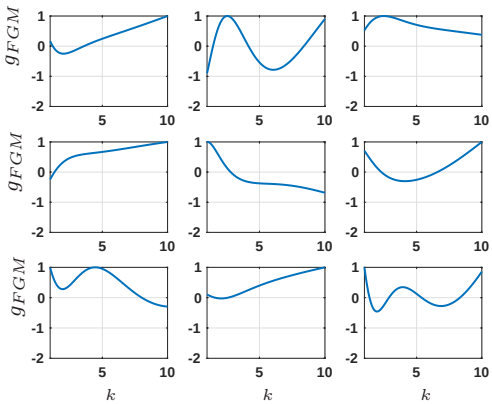

(b) functions g^i_{FGM} - i=10-18

Figure 4: functions $g^i_{FGM}(k)$ - one-layered - polynomial law

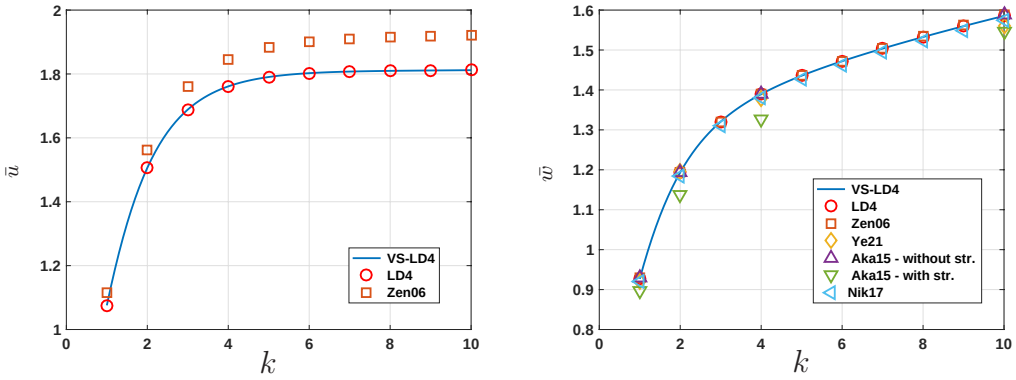

Figure 5: variation of the non-dimensional displacements $\bar{u}$ (left) and $\bar{w}$ (right) with respect to the volume fraction exponent k - S=10 - one-layered - polynomial law

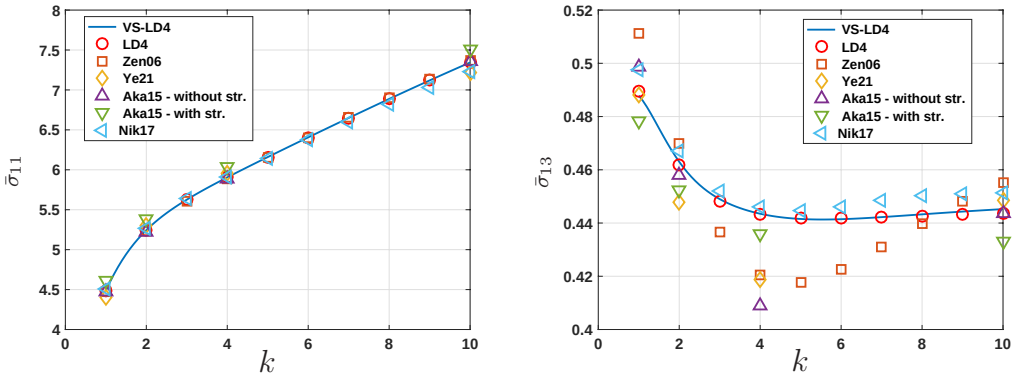

Figure 6: variation of the non-dimensional stresses $\bar{\sigma}_{11}$ (left) and $\bar{\sigma}_{13}$ (right) with respect to the volume fraction exponent k - S=10 - one-layered - polynomial law

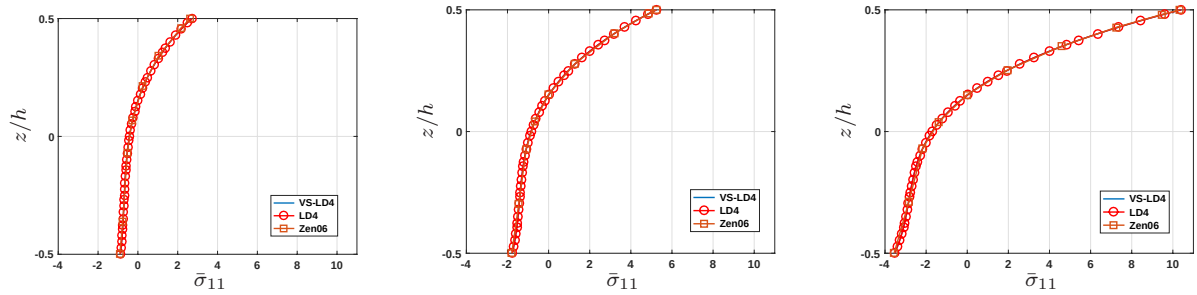

(a) $S = 5$ (b) $S = 10$ (c) $S = 20$

Figure 7: distribution of $\bar{\sigma}_{11}$ along the thickness - one-layered - polynomial law - $k = 2$

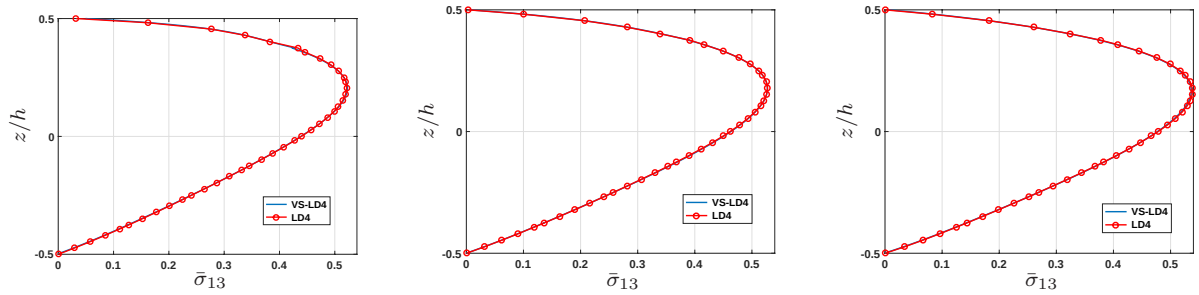

(a) $S = 5$ (b) $S = 10$ (c) $S = 20$

Figure 8: distribution of $\bar{\sigma}_{13}$ along the thickness - one-layered - polynomial law - $k = 2$

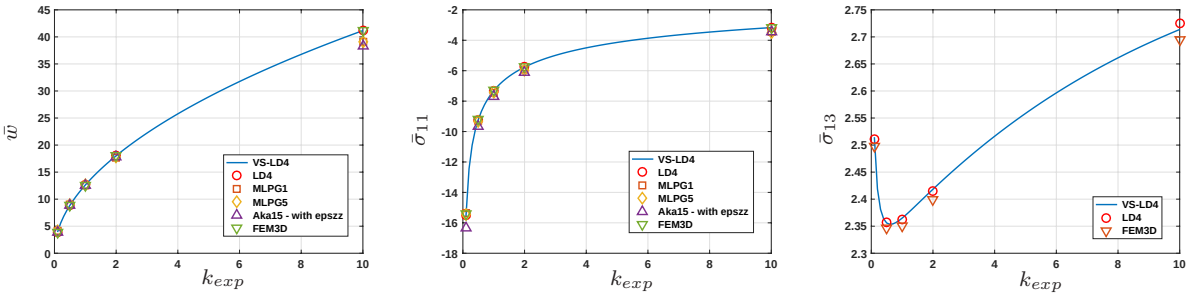

Figure 9: variation of the non-dimensional displacement $\bar{w}$ (left) and stresses $\bar{\sigma}_{11}$ (middle), $\bar{\sigma}_{13}$ (right) with respect to the volume fraction exponent $k_{exp} = E_t/E_b$ - S=5 - one-layered - exponential law

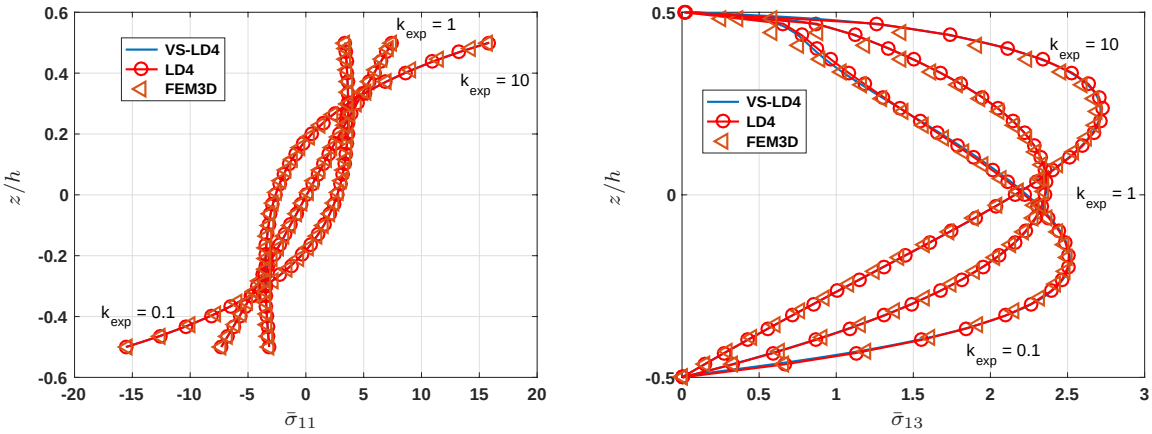

Figure 10: distribution of the non-dimensional stresses $\bar{\sigma}_{11}$ (left) and $\bar{\sigma}_{13}$ (right) along the thickness direction for different values of k_{exp} - S=5 - one-layered - exponential law

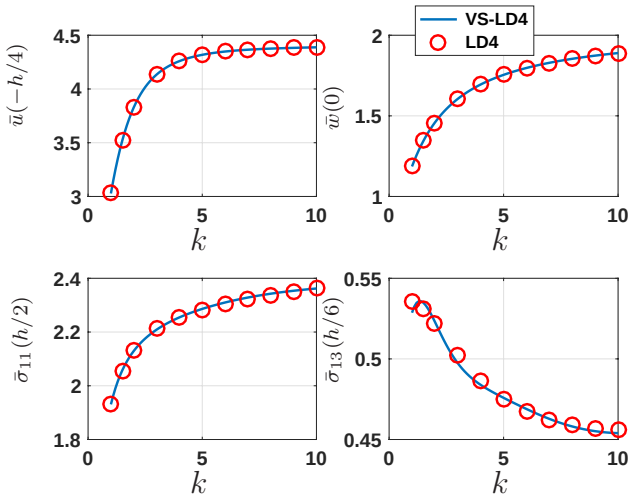

Figure 11: variation of the non-dimensional displacements $\bar{u}$, $\bar{w}$ and stresses $\bar{\sigma}_{11}$, $\bar{\sigma}_{13}$ with respect to the volume fraction exponent k - S=4 - Sandwich

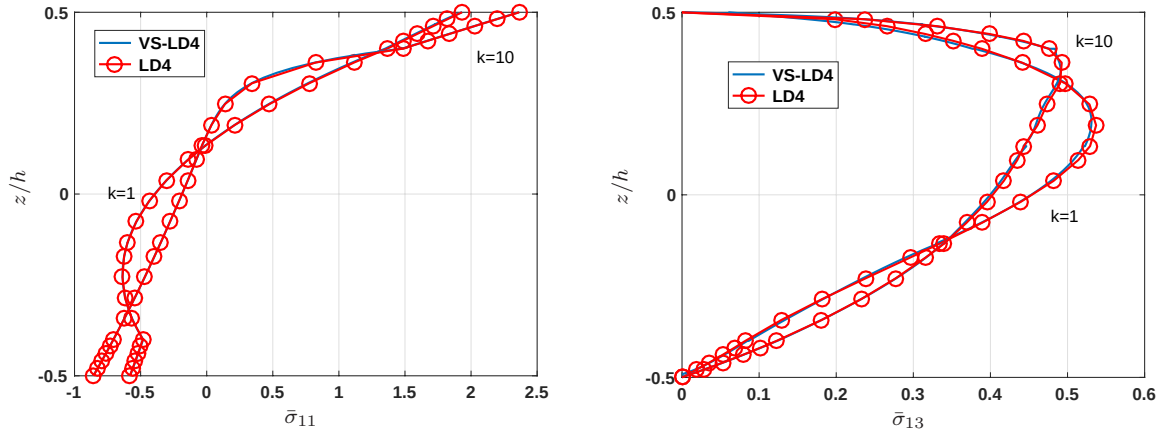

Figure 12: distribution of the non-dimensional stresses $\bar{\sigma}_{11}$ (left) and $\bar{\sigma}_{13}$ (right) along the thickness direction for two values of k (1, 10) - S=4 - Sandwich

List of Tables

[30]	LD4	Layerwise approach with a fourth-order z-expansion includind the stretching effect - 3D constitutive law - $12NC + 3$ unknown functions
[28]	Ye21	semi-analytical approach with the scaled boundary finite element method (SBFEM) using the 3D constitutive law - high order spectral elements with the order of 6 for the in-plane description
[19]	Zen06	HSDT model with a Sinus function involving 5 unknowns without stretching effect
[11]	Tha13	HSDT model with a Sinus function involving 4 unknowns without stretching effect
[46]	Nik17	Layerwise approach with Lagrangian linear functions for the z-coordinate - 3D constitutive law
[47]	Aka15 - $\varepsilon_{zz} = 0$	HSDT model with a hyperbolic shape function without stretching effect - 5 unknowns
[47]	Aka15 - $\varepsilon_{zz} \neq 0$	HSDT model with a hyperbolic shape function including the stretching effect - 6 unknowns
[48]	MLPG1	3D meshless local Petrov Galerkin approach considering a local weak formulation and using 3D constitutive law - fourth-order spline function as a test function
[48]	MLPG5	3D meshless local Petrov Galerkin approach considering a local weak formulation and using 3D constitutive law - Heaviside step function as a test function
[48]	FEM3D-Vag	3D FEM results from Ansys software using 36x36x36 SOLID45 elements

Table 1: Models available in open literature

k	N_{SVD}	$\bar{u}(-h/4)$	$\bar{w}(0)$	$\bar{\sigma}_{11}(h/3)$	$\bar{\sigma}_{13}(h/6)$
	1	4.2	1.7	15.7	29.2
	2	19.0	10.4	4.3	2.5
	3	3.3	2.1	0.1	0.2
1	4	0.9	0.6	0.0	2.1
	5	0.0	0.2	1.0	0.7
	6	0.1	0.3	0.7	0.3
	7	0.2	0.3	0.8	1.0
	8	0.1	0.1	0.3	0.1
	1	21.3	12.7	1.7	21.8
	2	10.2	4.6	7.2	5.3
	3	0.9	0.7	0.7	3.5
10	4	0.8	0.4	0.0	1.0
	5	0.1	0.1	0.1	0.0
	6	0.0	0.0	0.2	0.0
	7	0.0	0.0	0.1	0.1
	8	0.0	0.0	0.0	0.4

Table 2: convergence study on the number of the SVD (error rate [%]) - one-layered FGM plate - polynomial law - $b = a$ - $S = 10$ - $N_z = 8$

k	Model	$\bar{u}(-h/4)$	$\bar{w}(0)$	$\bar{\sigma}_{11}(h/2)$	$\bar{\sigma}_{13}(0)$
	VS-LD4	1.0756	0.9268	4.4837	0.4879
1	LD4	1.0757	0.9268	4.4839	0.4896
	Err	0.00	0.01	0.01	0.35
	VS-LD4	1.5061	1.1937	5.2441	0.4630
2	LD4	1.5060	1.1936	5.2442	0.4619
	Err	0.01	0.00	0.00	0.25
	VS-LD4	1.6886	1.3206	5.6261	0.4490
3	LD4	1.6886	1.3207	5.6272	0.4481
	Err	0.00	0.01	0.02	0.21
	VS-LD4	1.7612	1.3895	5.9053	0.4435
4	LD4	1.7611	1.3896	5.9050	0.4433
	Err	0.00	0.01	0.01	0.05
	VS-LD4	1.7905	1.4356	6.1593	0.4415
5	LD4	1.7904	1.4357	6.1583	0.4420
	Err	0.01	0.00	0.02	0.11
	VS-LD4	1.8025	1.4720	6.4062	0.4414
6	LD4	1.8025	1.4721	6.4056	0.4420
	Err	0.00	0.01	0.01	0.12
	VS-LD4	1.8075	1.5036	6.6490	0.4422
7	LD4	1.8075	1.5037	6.6491	0.4423
	Err	0.00	0.01	0.00	0.01
	VS-LD4	1.8097	1.5325	6.8871	0.4433
8	LD4	1.8098	1.5327	6.8877	0.4427
	Err	0.01	0.01	0.01	0.13
	VS-LD4	1.8109	1.5597	7.1191	0.4443
9	LD4	1.8110	1.5598	7.1199	0.4432
	Err	0.01	0.01	0.01	0.26
	VS-LD4	1.8119	1.5854	7.3439	0.4452
10	LD4	1.8120	1.5855	7.3446	0.4437
	Err	0.01	0.01	0.01	0.36

Table 3: comparison with LD4 model for different values of k - one-layered FGM plate - polynomial law - $b = a$ - $S = 10$ - $N_z = 8$

k	Model	$\bar{u}(-h/4)$	$\bar{w}(0)$	$\bar{\sigma}_{11}(h/2)$	$\bar{\sigma}_{13}(0)$
	VS-LD4	1.0756	0.9268	4.4837	0.4879
	Ye21	-	0.9212 (0.61)	4.4030 (1.80)	0.4882 (0.07)
1	Aka15 - $\varepsilon_{zz} = 0$	-	0.9288 (0.21)	4.4707 (0.29)	0.4988 (2.24)
	Aka15 - $\varepsilon_{zz} \neq 0$	-	0.8977 (3.14)	4.6110 (2.84)	0.4782 (1.98)
	Zen06 / Tha13	1.1153 (3.69)	0.9287 (0.20)	4.4745 (0.21)	0.5114 (4.82)
	Nik17	-	0.9203 (0.71)	4.5067 (0.51)	0.4976 (1.99)
	VS-LD4	1.5061	1.1937	5.2441	0.4630
	Ye21	-	1.1956 (0.16)	5.2970 (1.01)	0.4479 (3.26)
2	Aka15 - $\varepsilon_{zz} = 0$	-	1.1940 (0.03)	5.2248 (0.37)	0.4581 (1.06)
	Aka15 - $\varepsilon_{zz} \neq 0$	-	1.1376 (4.70)	5.3825 (2.64)	0.4524 (2.29)
	Zen06 / Tha13	1.5618 (3.70)	1.1940 (0.03)	5.2296 (0.28)	0.4700 (1.51)
	Nik17	-	1.1850 (0.73)	5.2656 (0.41)	0.4671 (0.89)
	VS-LD4	1.7612	1.3895	5.9053	0.4435
	Ye21	-	1.3779 (0.84)	5.9521 (0.79)	0.4187 (5.59)
4	Aka15 - $\varepsilon_{zz} = 0$	-	1.3888 (0.05)	5.8855 (0.34)	0.4090 (7.78)
	Aka15 - $\varepsilon_{zz} \neq 0$	-	1.3259 (4.58)	6.0382 (2.25)	0.4358 (1.73)
	Zen06 / Tha13	1.8439 (4.70)	1.3890 (0.04)	5.8915 (0.23)	0.4204 (5.21)
	Nik17	-	1.3800 (0.69)	5.9082 (0.05)	0.4460 (0.56)
	VS-LD4	1.8119	1.5854	7.3439	0.4452
	Ye21	-	1.5604 (1.58)	7.2217 (1.66)	0.4487 (0.78)
10	Aka15 - $\varepsilon_{zz} = 0$	-	1.5875 (0.13)	7.3617 (0.24)	0.4436 (0.37)
	Aka15 - $\varepsilon_{zz} \neq 0$	-	1.5453 (2.53)	7.5123 (2.29)	0.4332 (2.70)
	Zen06 / Tha13	1.9217 (6.06)	1.5876 (0.14)	7.3689 (0.34)	0.4552 (2.24)
	Nik17	-	1.5753 (0.64)	7.2262 (1.60)	0.4515 (1.41)

Table 4: comparison with models available in literature (% differences with respect to the VS-LD4 model in brackets) - one-layered FGM plate - polynomial law - $b = a$ - $S = 10$ - $N_z = 8$

$k_{exp} = E_t/E_b$	Model	$\bar{u}(-h/4)$	$\bar{w}_{max}$	$\bar{\sigma}_{11}(-h/2)$	$\bar{\sigma}_{13max}$
0.1	VS-LD4	0.1699 (1.36)	3.9182 (0.07)	-15.5725 (0.44)	2.5146 (0.17)
	MLPG1	-	4.0916 (4.49)	-15.3564 (0.96)	-
	MLPG5	-	4.1596 (6.23)	-15.4390 (0.43)	-
	Aka15 - $\varepsilon_{zz} \neq 0$	-	3.8333 (2.10)	-16.3220 (5.27)	-
	FEM3D-Vag	-	4.1215 (5.26)	-15.4030 (0.66)	-
	FEM3D	0.1675 (0.05)	3.9131 (0.06)	-15.4281 (0.50)	2.4982 (0.48)
	LD4	0.1676	3.9156	-15.5051	2.5103
0.5	VS-LD4	0.9609 (0.04)	8.8555 (0.01)	-9.2166 (0.06)	2.3560 (0.05)
	MLPG1	-	8.9751 (1.34)	-9.2902 (0.73)	-
	MLPG5	-	8.9357 (0.89)	-9.3279 (1.14)	-
	Aka15 - $\varepsilon_{zz} \neq 0$	-	8.8724 (0.18)	-9.6545 (4.68)	-
	FEM3D-Vag	-	9.0047 (1.67)	-9.2995 (0.83)	-
	FEM3D	0.9607 (0.05)	8.8524 (0.05)	-9.1982 (0.26)	2.3466 (0.45)
	LD4	0.9612	8.8568	-9.2226	2.3572
1	VS-LD4	1.7600 (0.04)	12.6174 (0.02)	-7.3143 (0.01)	2.3649 (0.13)
	MLPG1	-	12.5997 (0.12)	-7.4462 (1.81)	-
	MLPG5	-	12.6375 (0.18)	-7.4199 (1.45)	-
	Aka15 - $\varepsilon_{zz} \neq 0$	-	12.5970 (0.14)	-7.6944 (5.21)	-
	FEM3D-Vag	-	12.6133 (0.01)	-7.4588 (1.99)	-
	FEM3D	1.7584 (0.06)	12.6086 (0.05)	-7.3009 (0.17)	2.3500 (0.51)
	LD4	1.7594	12.6148	-7.3136	2.3619
2	VS-LD4	3.0717 (0.07)	18.0236 (0.07)	-5.7646 (0.11)	2.4184 (0.16)
	MLPG1	-	17.6640 (1.93)	-5.9410 (3.17)	-
	MLPG5	-	17.8397 (0.95)	-5.9711 (3.70)	-
	Aka15 -$\varepsilon_{zz} \neq 0$	-	17.7440 (1.48)	-6.1109 (6.12)	-
	FEM3D-Vag	-	17.7118 (1.66)	-5.9591 (3.49)	-
	FEM3D	3.0676 (0.06)	18.0023 (0.05)	-5.7533 (0.09)	2.3998 (0.61)
	LD4	3.0694	18.0113	-5.7583	2.4146
10	VS-LD4	9.7247 (0.23)	41.1617 (0.13)	-3.1671 (0.14)	2.7137 (0.40)
	MLPG1	-	39.0605 (5.23)	-3.4665 (9.30)	-
	MLPG5	-	39.0385 (5.28)	-3.4944 (10.18)	-
	Aka15 - $\varepsilon_{zz} \neq 0$	-	38.3330 (6.99)	-3.4530 (8.87)	-
	FEM3D-Vag	-	39.1558 (5.00)	-3.4805 (9.74)	-
	FEM3D	9.7400 (0.08)	41.1881 (0.06)	-3.1747 (0.10)	2.6951 (1.08)
	LD4	9.7474	41.2145	-3.1716	2.7246

Table 5: comparison with models available in literature (error rate in brackets) - one-layered FGM plate - exponential law - $b = a$ - $S = 5$ - $N_z = 16$

$k_{exp} = E_t/E_b$	Model	$\bar{u}(-h/4)$	$\bar{w}_{max}$	$\bar{\sigma}_{11}(-h/2)$	$\bar{\sigma}_{13\,max}$
	VS-LD4	0.0503 (0.87)	0.8732 (0.02)	-7.0855 (0.27)	1.5858 (0.46)
	MLPG1	-	0.9707 (11.18)	-7.2230 (2.22)	-
0.1	MLPG5	-	0.9688 (10.97)	-7.2034 (1.94)	-
	Aka15 - $\varepsilon_{zz} \neq 0$	-	0.8923 (2.20)	-7.6576 (8.37)	-
	FEM3D-Vag	-	0.9732 (11.47)	-7.2639 (2.80)	-
	FEM3D	0.0499 (0.01)	0.8728 (0.03)	-7.0330 (0.47)	1.5893 (0.24)
	exact	-	0.9731 (11.46)	-7.4555 (5.51)	-
	LD4	0.0499	0.8731	-7.0662	1.5931
	VS-LD4	0.2833 (0.01)	2.0650 (0.07)	-4.2021 (0.14)	1.5031 (0.24)
	MLPG1	-	2.1378 (3.45)	-4.3084 (2.38)	-
0.5	MLPG5	-	2.1498 (4.03)	-4.2943 (2.05)	-
	Aka15 - $\varepsilon_{zz} \neq 0$	-	2.0834 (0.82)	-4.5062 (7.09)	-
	FEM3D-Vag	-	2.1407 (3.59)	-4.3378 (3.08)	-
	FEM3D	0.2833 (0.02)	2.0661 (0.02)	-4.1978 (0.24)	1.5029 (0.25)
	exact	-	2.1402 (3.57)	-4.4149 (4.92)	-
	LD4	0.2834	2.0665	-4.2081	1.5066
	VS-LD4	0.5185 (0.05)	2.9813 (0.06)	-3.3208 (0.11)	1.5182 (0.21)
	MLPG1	-	2.9853 (0.19)	-3.4496 (3.77)	-
1	MLPG5	-	2.9603 (0.64)	-3.4959 (5.16)	-
	Aka15 - $\varepsilon_{zz} \neq 0$	-	2.9602 (0.65)	-3.5748 (7.53)	-
	FEM3D-Vag	-	2.9792 (0.01)	-3.4681 (4.32)	-
	FEM3D	0.5181 (0.03)	2.9790 (0.02)	-3.3192 (0.15)	1.5168 (0.30)
	exact	-	2.9795 (0.00)	-3.5176 (5.81)	-
	LD4	0.5182	2.9795	-3.3244	1.5214
	VS-LD4	0.9025 (0.02)	4.2825 (0.04)	-2.5953 (0.24)	1.5739 (0.01)
	MLPG1	-	4.1208 (3.74)	-2.7499 (5.70)	-
2	MLPG5	-	4.1098 (4.00)	-2.7556 (5.92)	-
	Aka15 - $\varepsilon_{zz} \neq 0$	-	4.1669 (2.66)	-2.8235 (8.53)	-
	FEM3D-Vag	-	4.1333 (3.45)	-2.7673 (6.37)	-
	FEM3D	0.9021 (0.03)	4.2801 (0.02)	-2.5999 (0.07)	1.5674 (0.40)
	exact	-	4.1320 (3.48)	-2.8041 (7.78)	-
	LD4	0.9024	4.2809	-2.6016	1.5737
	VS-LD4	2.8291 (0.24)	9.7369 (0.05)	-1.4091 (0.37)	1.8337 (0.13)
	MLPG1	-	8.7134 (10.47)	-1.6449 (17.16)	-
10	MLPG5	-	8.6923 (10.68)	-1.6566 (18.00)	-
	Aka15 - $\varepsilon_{zz} \neq 0$	-	8.9229 (8.31)	-1.5731 (12.05)	-
	FEM3D-Vag	-	8.7293 (10.30)	-1.6499 (17.52)	-
	FEM3D	2.8347 (0.04)	9.7296 (0.03)	-1.4057 (0.13)	1.8170 (0.78)
	exact	-	8.7303 (10.29)	-1.6724 (19.12)	-
	LD4	2.8358	9.7320	-1.4039	1.8313

Table 6: comparison with models available in literature (error rate in brackets) - one-layered FGM plate - exponential law - $b = a$ - $S = 10/3$ - $N_z = 16$